Egypt. J. Chem. Vol. 67, SI: M. R. Mahran, pp. **2161 - 2170** (2024)

Egyptian Journal of Chemistry

http://ejchem.journals.ekb.eg/

Controlled Release of Amoxicillin from Chitosan-Coated Poly(lactic-co-glycolic acid) Nanoparticles

Moshera Samy*, Magdy M. H. Ayoub

[1]*Polymers and Pigments Department, National Research Centre, 33 El Buhouth St., Dokki, Giza, 12622, Egypt*

Abstract

In this study, amoxicillin (AMX) loaded into poly (lactic-co-glycolic acid) nanoparticles (PLGANPs) were successfully prepared by the double emulsion technique using polaxamer 188 as a nonionic surfactant. We successfully coated the prepared nanoparticles (NPs) with different molecular weights of chitosan (CS). AMX-loaded PLGANPs were coated with CS in order to obtain controlled drug release and increase the bioavailability of AMX. The range of PLGANPs' entrapment efficiency (EE %) was determined to be between 74.39% and 85.63%. EE% showed a definite increase with increasing CS molecular weight. While TEM images revealed that the produced nanoparticles have a spherical form, CS-PLGANPs showed particles that were monodisperse and in the nanosize range. The zeta potential is changing from negative to positive. DSC, XRD, and FTIR confirmed AMX was fully encapsulated in PLGANPs and coated with CS. *In-vitro* AMX release from CS-PLGANPs showed sustained release, although slower release was observed when using CS with a higher molecular weight. According to research on drug release kinetics, CS-PLGANPs released AMX in a diffusion-controlled manner.

Keywords: Amoxicillin; Chitosan; Double emulsion; PLGA NPs; Sustained release.

.

1. Introduction

Among the penicillin family of antibiotics, amoxicillin (AMX) is a broad-spectrum lactam used for the treatment of many bacterial infections, including skin pneumonia, urinary infections, and throat infection [1, 2]. It has two basic components: an inner portion containing β-lactam and a side chain known as d-hydroxiphenilglicin [3]. Patients receive AMX at a dose of 250–500 mg every eight hours after being injected into the body. AMX works effectively when bacterial growth through bacterial growth, both gram-positive (*E. coli*) and gram-negative (*S. aureus and S. epidermidis*). AMX is one of the most common antibiotics for children. It was also used before surgery to prevent infections. From the digestive system, AMX is effectively absorbed [4]. However, AMX has an 8 hour half-life. The clearance of AMX is relatively quick in the body. AMX has disadvantages such as being expensive, having poor permeability across the mucus layer, having poor stability in the acidic pH of the stomach, and having poor bioavailability of sub-therapeutic antibiotic concentrations at the infection site afterward oral administration in tablet dose form oral traditional capsule, which results in taking a long time [5]. AMX entrapped into polymeric nanoparticles (PNPs) is one way to overcome these drawbacks. Solid nanocarriers known as PNPs are distinguished by having sizes smaller than 1 µm. Chemotherapeutic agents can be entrapped, attached, or dissolved within their matrices [6, 7]. These drug-based nanocarriers are unique in that it is simple to change their surface features and that they can protect and stabilize the drug they are carrying [8]. PNPs can also enable regulated release of drugs, promote tissue and cell selectivity, and increase drug bioavailability [9]. Biodegradable PNPs could regulate the medication concentration at the infection site, which would result in enhanced transport efficiency of drugs, enhanced drug bioavailability, extended drug residence time, reduced pollution, reduced dosages given, and reduced harmful side effects [10]. Nanoparticles prepared from poly (lactic-co-glycolic acid) (PLGA) are described to be safe and control the delivery of AMX. PLGA is a polymer that has obtained FDA permission due to its attractive physicochemical properties, excellent biocompatibility, and biodegradability [11]. Numerous studies have shown that PLGA has considerable promise as a carrier for drug delivery [12]. However, the potential for side effects as a result of drug burst release is one of PLGANPs' main drawbacks. Additionally, they are unable to precisely connect with proteins or cells, which prevents the accumulation of drugs in target areas. In order to get overcome these limitations, chitosan (CS) has been served as a coating material for PLGANPs [13]. CS is a natural cationic polysaccharide with biocompatibility, biodegradability, and nontoxicity. It is employed in a variety of products, including medicines, textiles, and tissue repairs. Generally, CS is thought to be nontoxic, biocompatible, and degradable[14]. Owing to CS its and biological adhesive physicochemical properties, where it has –OH and $–NH_2$ groups. Therefore, it has the ability for forming hydrogen and covalent bonding. Because low pH causes the $–NH_2$ groups to protonate, which charges the CS macromolecule positively, it eases the absorption of intracellular, improved membrane permeability drugs, and being flexible leads to the mucoladhesion of CS has attracted much research for the coating and modification of PLGANPs based drug delivery [15, 16]. Consequently, the current work intends to explore the double emulsion technique to create AMX loaded PLGANPs coated with CS

*Corresponding author e-mail: moshera_samy1984@yahoo.com (Moshera Samy)

Receive Date: 13 May 2024, Revise Date: 27 June 2024, Accept Date: 07 July 2024

DOI: 10.21608/ejchem.2024.272390.9703

of three different molecular weights. In this study, AMX served as a model drug entrapment efficiency, drug loading, and *in-vitro* drug released of CS-coated PLGANPs. We investigated the impact of CS molecular weight-coated PLGANPs on zeta potential, polydispersity index (PDI), and particle size. The thermal behavior and crystallinity were examined using thermal TGA and XRD, respectively. Additionally, using FTIR, DSC, and TEM, the incorporation of AMX into the produced CS-coated PLGANPs was assessed. Both the in vitro released pattern and the release kinetics studies of AMX from the produced nanoparticles were carried out.

2. Experimental

2.1. Materials

Poly (lactic-co-glycolic acid) (PLGA; with co-polymerization ratios 50:50 (lactic/glycolic); $(C_3H_4O_2)_x$ $(C_2H_2O_2)_y$; Mn 25000; product number 808482), Poloxamer 188 (F68) were obtained from Sigma-Aldrich, Germany. Three different molecular weights of chitosan (CS; $(C_6\ H_{11}NO_4)_n$; (1,4)-2-Amino-2-desoxy-beta-D-glucan),i.e., high, medium, and low (molecular weight 600000, 300000, and 150000 gm/mol, respectively), were obtained from Alfa Aesar, India. Amoxicillin (AMX) was purchased from laboratory NORMON, C. N. 694730 (Madrid, Spain). Dichloromethane (DCM; CH_2Cl_2; Mw = 84.93 g/mol; CAS: 75-09-2), disodium hydrogen orthophosphate (Na_2HPO_4) were delivered from Sigma-Aldrich, Germany. All chemical agents were of analytical grade.

2.2. Preparation of AMX loaded PLGANPs

Stock solutions of PLGANPs (2gm) were prepared by slowly adding into 100 mL DCM until fully dissolved with stirring till forming a clear solution. 30 mg/ml of AMX was dissolved in 1 ml of hot distilled H_2O in order to aid the dissolution of AMX and then 5 ml PLGA solution was added at constant (drug: polymer; 1:10). This mixture was properly homogenized using digital high speed homogenizer (T-10; model) at 20,000 rpm for 5 min using to get the primary emulsion (W1/O). Poloxamer 188 was added to deionized water (400 ml) to form the aqueous phase (0.3%, w/v). The aqueous Poloxamer 188 (0.3%, w/v) solution was mixed with organic solution with homogenization to achieve the double emulsion ($W_1/O/W_2$) [17, 18]. This mixture was properly homogenized at 21,000 rpm for 15 min by using digital high speed homogenizer (T-10; model). The organic solvent from the PLGA particles was made to diffuse more easily into the outer aqueous phase in the second step by using excess outer aqueous phase (W2). In order to eliminate all of the organic DCM, the resulting double emulsion (W1/O/W2) was evaporated under vacuum using a rotary evaporator (Heidolph type VV2000, type WB2000, Germany) [19].

2.3. Preparation of AMX loaded CS-coated PLGANPs

The NPs dispersions were mixed with an equivalent volume of three molecular weight of CS solution (2 mg/ml; 0.5% w/v acetic acid) under stirring for 2hr to allow the formation of CS-coated PLGA NPs. Under stirring for 2hr to allow the formation of CS-coated PLGANPs (CS-PLGANPs). The obtained PLGANPs were collected by centrifugation (K-2015 ambient centrifuge Centurion scientific, UK), at 6000 rpm at room temperature for 45 min and washed three times with water to remove excess coupling reagent. The obtained PLGANPs and CS-PLGANPs were stabilized using a freeze at −80 °C for three days and the powder was used for further analyses. All formulations were prepared in triplicate [20].

2.2. Analysis of AMX

2.2.1. Determination of the maximum absorption wavelength (λ_{max}) of AMX

Using AMX in water as a solvent, the spectrophotometric assay for AMX analysis was carried out using a Shimadzu UV spectrophotometer (2401/PC, Japan). With phosphate buffer saline (PBS) serving as a blank, the AMX dissolved in the studied solvent at 10 g/ml was screened to detect the λ_{max} of AMX from the UV spectrum. This concentration was made by diluting a stock solution of 10 µg/ml, which was made by properly weighing 10 mg of AMX and dissolving it in 10 ml of the PBS.

2.2.2. Formation of AMX calibration curve

Using the proper dilutions of the above-mentioned stock solution, eight concentrations of AMX 4, 6, 8, 10, 12, 14, 16, 18, and 20 µg/ml. were prepared in PBS as solvent. Each of these concentrations' absorbance was measured at the λ_{max} using PBS as a blank. The concentration of AMX and the UV absorbance at the appropriate wavelength of maximum AMX absorption in the water as a solvent were plotted on a linear calibration curve.

2.3. Characterization of PLGANPs and AMX loaded CS- PLGANPs

The PLGANPs and AMX-CS- PLGANPs were characterized based on size, charge, entrapment efficiency, PDI, FTIR, XRD, DSC, TGA surface morphology, the efficacy of AMX loading, and *in-vitro* release of AMX as drug model.

2.3.1. Determination of entrapment efficiency and drug loading

EE% of AMX in the prepared PLGANPs, the mixed washings was properly diluted with water after centrifugation. Using the regression equation of the standard calibration curve plotted using appropriate concentrations of AMX, the amount of free, unencapsulated AMX was determined spectrophotometrically at 228.18 nm. The amount of encapsulated AMX was determined by difference between the amount of unencapsulated, free AMX in the combined washings and the initial amount used in preparations of PLGANPs where the following equations was employed: EE% and DL% were calculated according to the following equations (1 and 2).

$$\mathbf{EE}\% = \frac{(\boldsymbol{AMX\ free - AMX\ total})}{\boldsymbol{AMX\ total}}\ \boldsymbol{X}\ \mathbf{100} \ldots (\mathbf{1})$$

$$\mathbf{DL}\% = \frac{\boldsymbol{Amount\ of\ entrapped\ AMX}}{\boldsymbol{Total\ weight}}\ \boldsymbol{X}\ \mathbf{100}.. (\mathbf{2})$$

AMXtotal is the amount of drug added, while **AMXfree** is the free amount of drug present the supernatant solution

.2.3.2. Determination of particle size (PS), polydispersity index (PDI) and zetapotential (ZP)

The PS, PDI and ZP for AMX loaded PLGA NPs and CS-PLGA NPs were measured by means of photon correlation spectroscopy (PCS) using a Zeta-sizer (Nano ZS, Malvern Instruments Ltd., Malvern, UK). Samples were suitably diluted with distilled water and measured at ambient temperature using quartz cuvettes. All experiments were done in triplicate and the results are expressed as mean ± standard deviation (SD).

2.3.3. FTIR

FTIR was used to study the chemical composition of PLGA, AMX, CS and freeze- dried AMX loaded PLGANPs and CS-PLGA NPs formulations. The spectra were recorded using FTIR spectrometer (Jasco, FT/IR 6100, Japan). The KBr pellet method was employed where the powdered samples were ground and mixed with KBr then compressed into discs. A scanning range of 4000–400 cm^{-1} was employed.

2.3.4. X-ray diffraction (XRD)

The physical state of AMX, PLGA, CS and freeze-dried AMX loaded CS-PLGANPs formulations was evaluated using X-ray diffraction. Measurements were acquired with X-ray diffractometer (Bruker AXS, D8 Advance, Germany) which was operated at 40 KV and 40 mA using CuK_α as a radiation source where λ=1.54 A°. The diffractograms were recorded in the diffraction angle (2θ) range between 5–60° and the process parameters were set at scan step size of 0.020° and scan step time of 0.4 s.

2.3.5. Thermal gravimetric analysis (TGA)

Thermal behavior for AMX, Low, Med, and High Mwt CS, PLGA and freeze-dried AMX loaded CS-coated PLGANPs samples was recorded using thermal analyzer TGA–SDT Q600 V20.9 Build 20, (USA) in the range from room temperature to 700°C at a heating rate of 10°C/min under inert nitrogen atmosphere (N_2) using referencealumina.

2.3.6. Differential scanning calorimetry (DSC)

Thermal analysis of AMX, (Low, Med& High Mwt) CS, PLGA and AMX -loaded CS-coated PLGANPs was performed by Perkin-Elmer Differential Scanning Calorimeter (Shimadzu, DSC-60, Japan). The samples were scanned at a temperature that ranged from 20°C to 400°C, with a scan rate of 10°C/min and the analysis took place in aluminum pans, under nitrogen atmosphere using reference alumina.

2.3.7. Transmission electron microscopy (TEM)

The morphology of AMX-loaded PLGA NPs and AMX-loaded CS coated PLGA NPs formulations and their dimensions in nanometer range was confirmed by transmission electron microscopy. The TEM (JEOL Co., JEM-2100, Japan) was adjusted at a high tension electricity of 200 kV. One drop of the appropriately diluted sample was placed onto a carbon-coated copper grid, negatively stained with 1% phosphotungstic acid and left to dry at ambient temperature before being examined at suitable magnifications.

2.3.8. *In-vitro* drug release study

The *in-vitro* release of AMX from prepared CS-PLGANPs, was evaluated employing the dialysis bag technique employing a dialysis tubing cellulose membrane (Visking R, SERVA Electrophoresis GmbH, Germany; Molecular weight cut of 12.000–14.000). An amount equivalent to 2 mg of AMX was instilled in the dialysis bag, sealed at both ends to prevent leakage and placed in screw capped glass containers filled with 50 ml phosphate buffer solution (PBS) (pH 7.4). The release of AMX was calculated based on a standard AMX absorbance concentration calibration curve at 228.18 nm [21] . The entire system was kept at 37 ± 0.5 °C at 100 rpm using a shaking water bath. At predetermined time intervals (1, 2, 3, 4, 6, 8, 24 and 48 h), 5 ml of the release medium was withdrawn and replaced with 5 ml of fresh PBS. The samples were adequately diluted and analyzed for AMX content spectrophotometrically at 228.18 nm. The cumulative percentage of drug released was determined as the ratio of the amount of released AMX to the amount of AMX initially inserted into the dialysis bag was calculated by using following equation (eq.3)[22]. All measurements were performed in triplicates.

$$\textbf{Drug release}\% = \frac{\boldsymbol{Amount\ of\ AMX\ released}}{\boldsymbol{Amount\ of\ AMX\ loaded}}\ \boldsymbol{X}\ \mathbf{100}\ldots(\mathbf{3})$$

2.3.9. Drug release kinetics and mechanism

Kinetic analysis of drug release of AMX from different CS-coated PLGANPs was performed using various mathematical models such as zero order and first order models as well as Higuchi's model, Hixson-Crowell cube root law, Baker-Lonsdale equation of time kinetics and Peppas exponential model [23]. The regression coefficient values (R^2) were calculated from the plots of Q vs. t .

Zero order and first order Kinetics are used to determine the rate of water soluble drug diffusion from the drug delivery system which depends on time and concentration, respectively.

The mathematical expression for the kinetics are as follows.

Zero order: $Q_t = Q_0 + K_0\ t$ (4)

First order: $\log Q_t = \log Q_0 + K_1\ t/2.303$ (5)

Where, $\mathbf{Q_t}$ is the percentage of released drug at time t, $\mathbf{Q_0}$ is the initial amount of drug, $\mathbf{K_0}$ and $\mathbf{K_1}$ is the zero and first order released constant, respectively. Pappas mathematical expression gives us the prediction of mechanism of drug diffusion from the drug delivery system. The system may follow Fickian and non-Fickian diffusion mechanism regardless of the drug delivery system.

Peppas model: $\log (Q_t/Q_0) = \log K + n \log t$ (6)

Where, Q_t/Q_0 is the amount of fractional drug released at time t, **K** is the constant which depends on the structure and geometry of the drug carrier and **n** represents release exponent was also calculated in ordor to determine drug release mechanism [24].

Higuchi model describes about the released mechanism of drugs (both water soluble and poorly soluble) from the carrier and the respective mathematical expression is as follows.

Higuchi model: $Q_t = Q_0 + K_H t^{1/2}$ (7)

Where, Q_t is the amount drug released at time t, Q_0 is the initial amount of drug, K_H and K_1 is rate constant.

Hixson-Crowell model: $Q_0^{1/3} - Q_t^{1/3} = kt$ (8)

Baker-Lonsdale model:

$$Q_0^{3/2}[1-(1-Q_t/Q_\infty)^{2/3}]-Q_t/Q_0 = kt \quad (9)$$

Where **k** is the release constant corresponds to the slope. This equation can be used to the linearization of the release data from several formulations of nanoparticles.

2.3.10. Statistical analysis

The experimental results were presented as mean value ±standard deviations (SD). Statistical analysis was performed by means of a two-way analysis of variance (ANOVA). All experiments were repeated at least three times. The statistical significance of the differences was evaluated by two-way analysis of variance and $P<0.05$ was considered to indicate a statistically significant difference.

3. Results and discussion

3.1. Preparation of AMX Loaded CS-coated PLGANPs

PLGANPs were prepared via the double emulsion method, where the electrostatic interaction of negatively charged PLGA chains caused CS, to dissolve in the aqueous phase and soak onto the surfaces of the PLGANPs. Utilizing cationic CS. The obtained NPs can be modified by covalent binding techniques, copolymerization, absorption, or integration. Since the absorption strategy can be used without the use of costly and hazardous coupling chemicals, it was selected for our study. The surfaces of the NPs were coated with CS with three different molecular weights in order to obtain controlled drug release as compared with brust release of PLGANPs, according to literature. Figure 1 demonstrates how the double emulsion method was used to successfully synthesized AMX loaded CS coated PLGANPs in the nanoscale range. The proposed formulation of CS coated PLGANPs loaded with AMX is shown in Table (1).

Table 1: EE%, DL%, PS, PDI and ZP of AMX loaded PLGANPs.

Formulations	CsMwt	AMX (mg/ml)	EE%	DL%	PS(nm)	PDI	ZP (mV)
AMX- PLGANPs	-	30	-	-	216.7 ±1.37nm	0.11	-2.7 ± 0.1 mV
AMX-CSL-PLGANPs	LOW	30	85.63%	47.36%	254.76±1.14nm	0.07	+48.1 ± 5.3mV
AMX-CSM- PLGANPs	Med	30	74.39%	34.61%	270.43±1.19 nm	0.16	+37.5 ±1.9 mV
AMX-CSH-P LGANPs	High	30	80.31%	41.9%	280.62±1.28nm	0.18	+33.26 ± 1.0 mV

The results are shown as mean ± standard deviation where, n = 3.

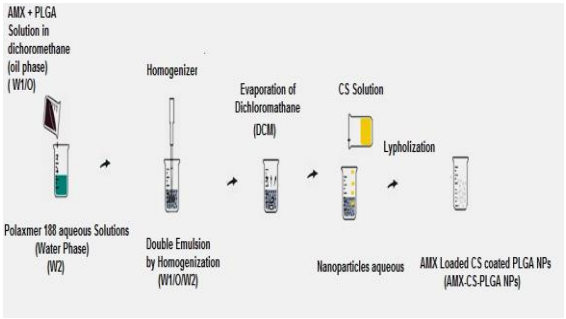

Figure (1): Schematic presentation for preparation of AMX loaded CS-coated PLGANPs prepared by double emulsion technique

3.2. AMX essay

3.2.1. AMX analysis method

Screening AMX in water with a pH of 7.4 across a UV spectroscopic scan (200-400 nm) was the first step in determining the λ_{max} of AMX. As shown in Figure 2, the stock solution of 10 µg/ml and various concentrations of AMX of 4, 6, 8, 10, 12, 14, 16, 18, and 20 µg/ml were diluted in PBS to produce standard solutions in the range of 4-20 µg/ml. Each of these concentrations' absorbance was measured at λ_{max} for the PBS.

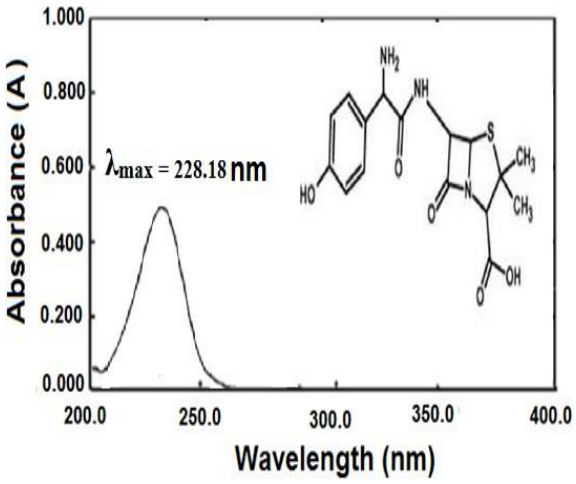

Figure (2): UV absorbance spectrum of AMX in PBS

3.2.2. Calibration curve of AMX

Using the X and Y axes to plot the concentration and absorbance, a calibration curve for the concentration range of 4-20 µg/ml was created in supplementary Figure 1. The assay for detecting the concentration of AMX was determined to be accurate and reliable because the λmax of was reported to be 228.18nm[25, 26] by using PBS as blank[17]. A good linearity was obtained between UV absorbance values and AMX concentrations via regression equations (Y= 0.0235X+0.0072) and linear regression, which had a correlation coefficient R^2 of 0.9993. The slope

was calculated to be 0.0235 which confirmed the assay′s reliability and accuracy in estimating AMX concentrations.

3.3. Characterization of poly (lactic-co-glycolic acid) nanoparticles

3.3.1. Drug Entrapment efficiency (EE%) and drug loading (DL%)

EE% indicates a vital parameter for the assessment of PLGANPs as nanocarrier. EE% is influenced by a number of factors, including drug content, CS molecular weight, CS concentration, and production technique and production technique. The EE% of AMX loaded CS-PLGANPs formulation is displayed in Table 1. According to the findings, PLGANPs had EE% values ranging from 74.39% to 85.63% [27]. The increase in CS Mwt measured makes it obvious that an increase in EE% was noted. According to these findings, CS coated PLGANPs have greater EE% and DL% than other PLGANPs formulations under investigation. The surface coating of PLGANPs with CS may be responsible for the increase in EE%. Additionally, the significant DL% demonstrates that AMX was absorbed onto the surface of PLGANPs following interaction between +Ve charged CS and -Ve AMX. This finding agrees with Badran *et al.* [28] and Al-Nemrawi *et al.* [27].

3.3.2. PS, PDI and ZP

Table 1 displays the findings of measuring PS values for the created PLGANPs formulations. The findings demonstrate that all of the formulations put to the test were in the nanosize range, with PS falling between 216.7 and 280.62 nm. As higher molecular weight CS, PS of PLGANPs increased. The findings show that PS of PLGANPs was significantly influenced by CS Mwt this agree with literature [29]. As greater molecular weight CS was employed, PS of PLGANPs rose. The findings show that PS of PLGANPs was significantly influenced by Mwt of CS this fits the literature. A homogeneous size distribution is shown by indicates Monodisperse colloidal dispersions. ZP assessment used to investigate the physical stability. According to the findings, the obtained PLGANPs had a negative ZP (-2.7±0.1mV) is possibly attributed to the presence of PLGA's ionized carboxyl group while the AMX-CS-PLGA NPs nanoparticles had positive charges. Nanoparticles that were prepared using low, med, and high of CS gave particles with average charges of +48.1 ±5.3 mV, +37.5 ± 1.9 mV, and +33.26 ± 1.0 mV, respectively. As can be observed in Table 1, the surfacecharge was discovered to be unrelated to the CS molecular weight. Although evidence of a successful coating was supplied by changes in the surface charges after the PLGANPs were coated with CS. Similar results were also reported for other drug CS coated NPs [29, 30].

3.3.3. FTIR analysis

FTIR spectra of AMX, Low, Med, and High Mwt CS, PLGA and AMX-loaded PLGANPs at three different Mwt CS (AMX-CS$_L$-PLGANPs, AMX-CS$_M$-PLGANPs &AMX-CS$_H$-PLGANPs) as shown in Figure 3. FTIR spectra of AMX showed a band was showed at 1685.13 cm^{-1} owing to C=O stretching of amide and peaks at 1577.24 cm^{-1} represents asymmetric COO stretching [31]. band at 3443.22 cm^{-1}, representing N-H, O-H stretching frequencies and other representative peaks at 1772.51 cm^{-1} which can be assigned to C=O stretching of β-lactamic. The characteristic vibrational peak at 655.49 cm^{-1} (C-S) [32, 33]. The N-H bending of amide II and amide I in FTIR of LOW, Med, and High Mwt CS, respectively, is what provides the intense peaks at 1647.8, 1604.3 cm^{-1}, 1646.6, 1602.7 cm^{-1}, and 1648.9,1605.5 cm^{-1}. The chemical structures of low, medium, and high molecular weight CS each have typical C-N absorption bands extending at 2881.1, 2880.1, and 2919.7 cm^{-1}, respectively [34]. FTIR spectrum of PLGA shows peaks at 1745.23 cm^{-1} (C=O stretching vibration), 691.3 cm^{-1} (-CH stretching frequencies), at 1511.9 cm^{-1} (-CH$_3$ stretching frequencies), 1027.8-1186.01 cm^{-1} (C-O stretching vibrations associated with ester groups were assigned to asymmetric and symmetric C-C-(C=O-O stretches in both the lactide and glycolide monomers, 2931.2-2850.1 cm^{-1} (C-H stretching vibrations), and 3200 - 3600 cm^{-1} (OH group)[35]. Concerning the FTIR spectra of AMX-CS$_L$-PLGANPs, AMX-CS$_M$-PLGANPs and AMX-CS$_H$-PLGANPs shows peaks at 3457.33 cm^{-1} (NH$_2$), 2953.40 cm^{-1} (NH), 1727.56 cm^{-1} (C=O), 940.54 cm^{-1} (C-O-C). 2931.2-2850.1 cm^{-1} (-CH stretching frequencies),1577.24 cm^{-1} (amide group and C-H stretching in CS), and 3200-3600 cm^{-1} (-NH$_2$ and O-H stretching vibration of CS) [13]. The CS distinguishing peaks were obtained in chemical structure of CS-coated PLGANPs. Furthermore, the presence of the distinctive AMX peaks, which indicate the interaction of AMX with CS-PLGA molecular structures and hence successful loading of AMX into the produced nanoparticle, could be seen.

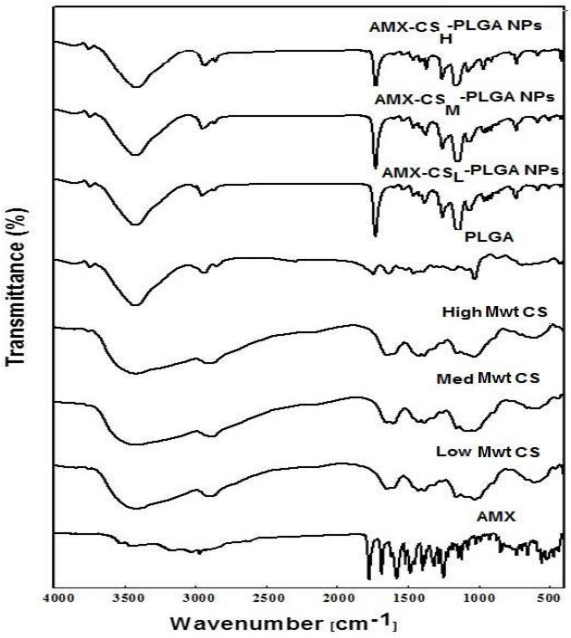

Figure (3) FTIR spectra of AMX, Low, Med, and High Mwt CS, PLGA, and AMX-CS-PLGANPs (AMX-CS$_L$-PLGANPs, AMX-CS$_M$- PLGANPs & AMX-CS$_H$-PLGANPs)

3.3.4. XRD

The amorphous or crystalline nature of the AMX loaded CS coated PLGA nanoparticles were investigated using XRD. The XRD patterns of AMX, Low, Med, and high Mwt CS, PLGA and AMX-CS-PLGANPs (AMX-CS_L-PLGANPs, AMX-CS_M-PLGANPs & AMX-CS_H-PLGANPs) are presented in figure 4. The XRD patterns of pure AMX exhibited a number of peaks at 2θ values of 12.18°, 15.15°, 16.26°, 18.06°, 19.35°, 20.21°, 26.70°, 28.72° and 29.49°. Almost similar peaks have also been described by Singh M *et al*. [36]. Strong diffraction peaks were visible in the diffraction patterns of low, medium, and high molecular weight CS at 2θ =10.8, 19.9°, 11.3°, 19.9°, 20.3°, and 22.09° indicating the crystalline structure of CS[37]. PLGA's XRD showed no sharp peaks, indicating that it is amorphous[38]. These results also confirmed that the AMX particles existed in CS-PLGA matrix. Vanishing of the characteristic peaks of AMX in the spectra of AMX loaded CS-PLGANPs fully encapsulated and coated with the polymers in an amorphous state [39]. Other drugs that were encapsulated in CS-PLGANPs exhibited similar outcomes[40].

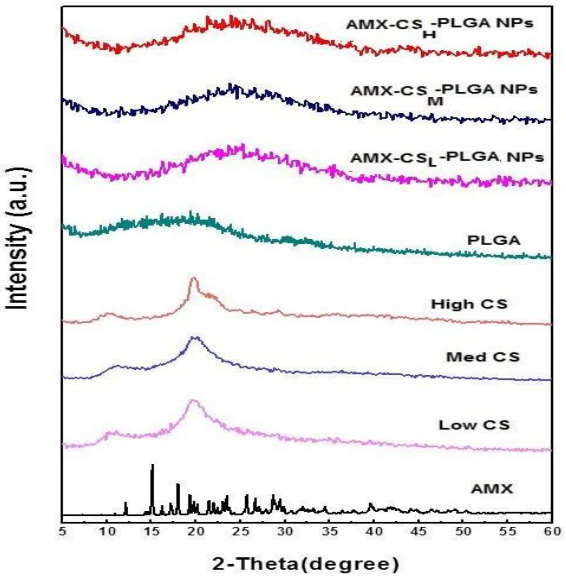

Figure (4): XRD diffractograms of AMX, Low, Med, and High Mwt CS, PLGA, and AMX-CS-PLGANPs (AMX-CS_L-PLGANPs, AMX-CS_M- PLGANPs & AMX-CS_H-PLGANPs)

3.3.5. DSC

DSC thermograms of AMX, Low, Med, and High Mwt CS, PLGA, AMX loaded CS-coated PLGANPs formulations and their individual components are presented in Figure 5. When drug loaded into PNPs, the DSC technique can reveal information about the drug's physical and chemical properties [41]. The final melting temperature (t_m) and enthalpy variation (H) derived from DSC curves are shown in Figure (6). AMX exhibits 1st endo thermic peak appeared at 120.1°C which attribute to AMX dehydration. The 2nd and 3rd endothermic peaks appeared at peaks appeared at 180.0˚C and 322.3˚C attributed to the amoxicillin fusion degradation event (ΔH = −68.13 j/ g and −24.53 j/g, respectively). Also, AMX DSC curve displays an exothermic at 240.6 °C represent the AMX transition into the crystal state [42]. According to DSC of PLGA, T_g of PLGA was 74.34 ºC. Exothermic peaks can be seen on the DSC thermograms of Low, Med & High Mwt CS respectively, at temperatures of 309.63, 308.64, and 304.18°C. It is believed that the temperature at which the polysaccride decomposes is what causes these exothermic peak[43]. The distinctive peak for AMX vanished, according to DSC thermograms of the CS-coated PLGANPs formulations AMX-CS_L-PLGANPs, AMX-CS_M- PLGANPs & AMX-CS_H-PLGANPs. Such results have been previously reported [39], and may be caused by the drug's molecular dispersion within the nanoparticles.

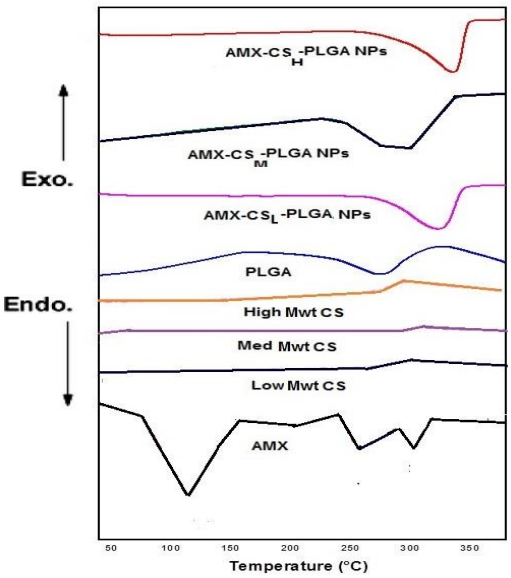

Figure (5): DSC thermograms of of AMX, Low, Med, and High Mwt CS, PLGA, and AMX-CS-PLGANPs (AMX-CS_L-PLGANPs, AMX-CS_M- PLGANPs, and AMX-CS_H-PLGANPs

3.3.6. TGA

Figure 6 showed thermal decomposition of AMX occurred in two degradation stages in the range of 46-224 ºC; 224-500 ºC with weight of 0.7, 83.78%, respectively due to water loss. CS have thermal decomposition occurred in two stages. The first occurring in the range of 46.1-240 ºC; 46.1-220 ºC; 46.1-230 ºC, for Low, Med, and High Mwt CS lost due to thermal degradation with a weight loss of about 5% loss of water molecules and second degradation with a weight loss of water molecules and second degradation at 29-200ºC. PLGA was thermally stable until 200 ºC due to thermal degradation with a weight loss 3.88% where the thermal decomposition occurred in one stage at 200-381 ºC with weight loss of 4.02%. The decomposition products of PLGA are comparable to those of neat PLA and PLGA polymers [44]. For AMX-CS-PLGANPs were degrade at 322 ºC instead of 46 ºC for pure AMX which was ascribed to CS-PLGA presence that an improvement in thermal stability of AMX-CS-PLGA compared to pure AMX. Which confirmed that the AMX fully encapsulated in PLGANPs and coated with CS. Similar results obtained from FTIR and XRD.

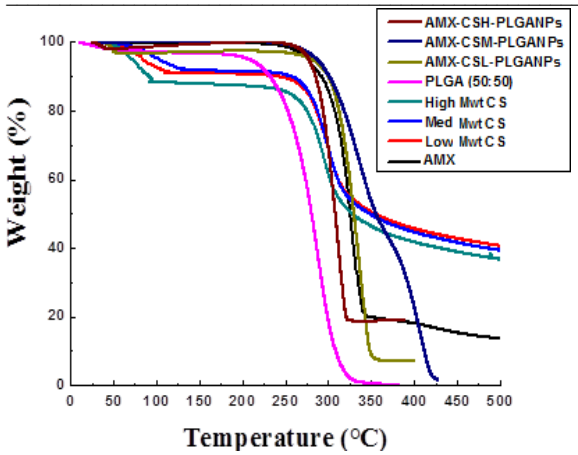

Figure (6): TGA thermograms of AMX, Low, Med, and High Mwt CS, PLGA, and AMX-CS-PLGANPs (AMX-CS_L-PLGANPs, AMX-CS_M- PLGANPs &AMX-CS_H-PLGANPs) at a heating rate of 10 °C / min

3.3.7. TEM

TEM is very important characterization technique which was used to investigate formulations shape of AMX-CS-PLGANPs formulations as AMX-CS_L-PLGANPs, AMX-CS_M-PLGANPs and AMX-CS_H-PLGANPs at Low, Med and High Mwt CS, respectively as shown in Figure 7. According to the micrographs, the obtained nanoparticles were spherical and had a narrow size distribution. They did not aggregate with core shell which confirmed the AMX entrapment. Their diameters appeared to be consistent with finding of the PS investigation.

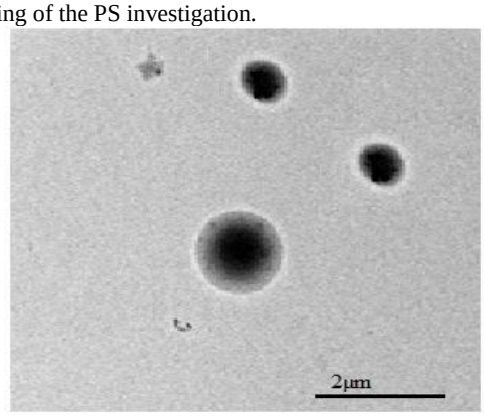

AMX-CSL-PLGANPs

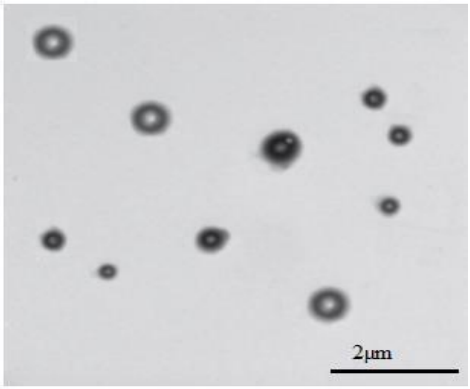

AMX-CSM-PLGANPs

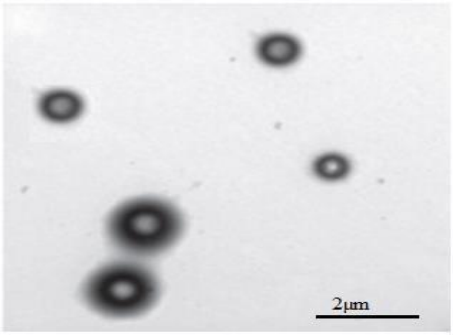

AMX-CSH-PLGANPs

Figure (7): TEM photos of AMX-CS-PLGANPs (AMX-CS_L-PLGANPs, AMX-CS_M-PLGANPs and AMX-CS_H-PLGANPs)

.3.3.8In vitro drug release

In comparison to the free drug suspension, Figure 8 describes the in-vitro release profile of AMX from three CS coated PLGNPNPs formulations: AMX-CSL-PLGANPs, AMX-CSM-PLGANPs & AMX-CSH-PLGANPs. The percentage of AMX released after 48 hours was 82.48%, 80.37%, and 77.48% for AMX-CSL-PLGANPs, AMX-CSM-PLGANPs, and AMX-CSH-PLGANPs, respectively, for all three CS-PLGANPs formulations. On the other hand, AMX suspension demonstrated a relatively fast release, reaching 94.07% in just 6 hrs (Table 2). The profiles of release the CS-coated PLGANPs formulation under investigation exhibited a biphasic tendency, with an initial fast release occurring during the first hour. Following that, there was a slow, sustained released for 8 hours, it could be explained by the strong hydrogen connection between CS and AMX, which prevents AMX dispersing into the release medium. Moreover, after 48 hours, the percentage of medication that was released considerably increased ($P<0.05$) as the CS Mwt decreased. Similar pattern in relation to CS Mwt was observed in case CS-coated PLGANPs, where AMX-CSL-PLGANPs was connected to a more sustained release profile[45, 46].

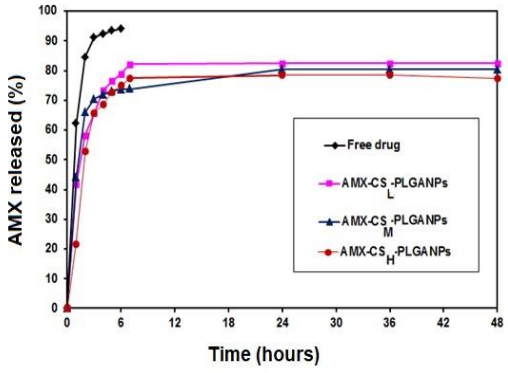

Figure (8): *In-vitro* release profiles of free AMX and AMX-CS-PLGANPs formulations (AMX-CS_L-PLGANPs, AMX-CS_M-PLGANPs & AMX-CS_H- PLGANPs) in PBS, pH 7.4 at 37 °C.

3.3.9. Drug release kinetics

The study of drug release kinetics and mathematical models are important for the estimate of drug release rate and the mechanism followed by the drug delivery system. When compared to the other derived mathematical models, the zero order model which reveals that the AMX diffuses in a controlled manner with respect to time as observed from highest R^2 for the release pattern of the CS-coated PLGANPs formulations under investigation (Table 2). According to this findings, the CS- coated PLGANPs exhibit diffusion–based release Kinetics, which is consistent with other results on CS- coated PLGANPs. The data of release using Peppas eq. and release exponents "n" was done in order to better elucidate the mechanism of drug release . Peppas's theory states that drug release correspond to the Fickian diffusion mechanism if n≤0.43. The release correspond to anomalous (non-Fickian) diffusion n is between 0.43 and 0.85. When n equal to 0.85, case II transport. The values of the release exponent "n" was less than or equal to 0.43 as shown in Table 2, which points to a Fickian release mechanism. This provides additional evidence that a diffusion process mainly controlled the release of AMX from CS-coated PLGANPs.

Table 2: kinetics parameters and the calculated R^2 of AMX *in-vitro* release profile from CS-coated PLGANPs formulations.

Formulations	Q48h (%±S.D.)	Zero order	First order	Higuchi	Hixon Crowell	Baker Lonsdale	Peppas	
		R^2					R^2	n
AMX-CS_L-PLGANPs	82.48± 6.72	0.9367	0.8789	0.8824	0.8832	0.8742	0.8712	0.2053
AMX-CS_M-PLGANPs	80.37± 5.48	0.8952	0.8646	0.8680	0.8697	0.8863	0.7892	0.1017
AMX-CS_H-PLGANPs	77.48± 3.73	0.9637	0.8783	0.9126	0.9033	0.9460	0.8635	0.1323

Q48h: Percent total AMX released after 48 h

4. Conclusion

Polymeric nanoparticles based drug delivery are a promising method that clearly outperforms traditional dosage forms owing to they have the ability to increase permeability and bioavailability of AMX. In this study, AMX loaded chitosan-coated PLGA nanoparticles were prepared via double emulsion technique where a the molecular weight of CS that influence characteristics of the nanoparticles were investigated in order to obtained controlled drug release and increase bioavailability of AMX. Both EE% and PS of the prepared PLGANPs formulations exhibited decrease, an increase, respectively with increasing the CS molecular weight. The AMX-CS_L-PLGANPs exhibited the highest EE% with low PS in the nanorange.

The changing in ZP values from negative to positive confirmed the successful PLGA nanoparticles coated by chitosan. According to TEM, A spherical shape could be seen in nanoparticles. The results of FTIR, TGA, and XRD investigations confirmed successful entrapment of AMX within the prepared CS-coated PLGANPs. A diffusion-based kinetic model was used to predict the biphasic release of AMX from CS-coated PLGANPs. Moreover, AMX-CS_H-PLGANPs using lower molecular weight CS resulted in higher drug release. According to all previous findings. Mw of chitosan significant influence on the nanoparticle properties and governing the successful formulation of PLGANPs as suitable carrier for efficient delivery of AMX. Based upon these findings we conclude chitosan--coated PLGANPs could be promising candidate for AMX delivery.

Supplementary data

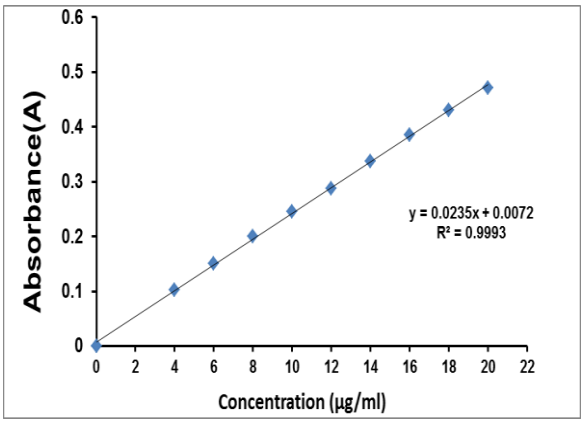

Supplementary Figure (1): Calibration curve of AMX of in water (UV absorbance as function in concentration)

Data availability

The raw data required to reproduce these findings are available from thecorresponding author upon request.

Declaration of interest

The author report no declarations of interest.

References

1. Mosavi SS, Zare EN, Behniafar H, Tajbakhsh M. Removal of amoxicillin antibiotic from polluted water by a magnetic bionanocomposite based on carboxymethyl tragacanth gum-grafted-polyaniline. Water. 2023;15(1):202.
2. Garnier A-S, Drablier G, Briet M, Augusto J-F. Nephrotoxicity of amoxicillin and third-generation cephalosporins: an updated review. Drug Safety. 2023;46(8):715-24.

3. Ecke A, Schneider RJ. Pitfalls in the immunochemical determination of β-lactam antibiotics in water. Antibiotics. 2021;10(3):298.
4. Metheeparakornchai C, Kreua-ongarjnukool N, Thumsing S, Pavasant P, Limjeerajarus C. Development of amoxicillin-loaded modified polycaprolactone microparticles in medical application. International Journal of Pharma Medicine and Biological Sciences. 2021;10(2):88-93.
5. Pooresmaeil M, Namazi H. Chitosan coated Fe3O4@ Cd-MOF microspheres as an effective adsorbent for the removal of the amoxicillin from aqueous solution. International Journal of Biological Macromolecules. 2021;191:108-17.
6. Amin A, Samy M, Abd El-Alim SH, Rabia AEG, Ayoub MM. Assessment of formulation parameters needed for successful vitamin C entrapped polycaprolactone nanoparticles. International Journal of Polymeric Materials and Polymeric Biomaterials. 2018;67(16):942-50.
7. Othman R, Vladisavljević GT, Nagy ZK. Preparation of biodegradable polymeric nanoparticles for pharmaceutical applications using glass capillary microfluidics. Chemical Engineering Science. 2015;137:119-30.
8. Sahle FF, Balzus B, Gerecke C, Kleuser B, Bodmeier R. Formulation and in vitro evaluation of polymeric enteric nanoparticles as dermal carriers with pH-dependent targeting potential. European Journal of Pharmaceutical Sciences. 2016;92:98-109.
9. Mora-Huertas CE, Fessi H, Elaissari A. Polymer-based nanocapsules for drug delivery. International journal of pharmaceutics. 2010;385(1-2):113-42.
10. Zhao Z, Han J, Xu S, Jin Z, Yin TH, Zhao K. Amoxicillin encapsulated in the N-2-hydroxypropyl trimethyl ammonium chloride chitosan and N, O-carboxymethyl chitosan nanoparticles: Preparation, characterization, and antibacterial activity. International Journal of Biological Macromolecules. 2022;221:613-22.
11. Choi J-S, Park J-S. Design and evaluation of the anticancer activity of paclitaxel-loaded anisotropic-poly (lactic-co-glycolic acid) nanoparticles with PEGylated chitosan surface modifications. International Journal of Biological Macromolecules. 2020;162:1064-75.
12. Macedo LB, Codevilla CF, Mathes D, Maia BC, Rolim CMB, Nogueira-Librelotto DR. Biofate and cellular interactions of PLGA nanoparticles. Poly (lactic-co-glycolic acid)(PLGA) Nanoparticles for Drug Delivery: Elsevier; 2023. p. 87-119.
13. Lu B, Lv X, Le Y. Chitosan-modified PLGA nanoparticles for control-released drug delivery. Polymers. 2019;11(2):304.
14. Sahdev AK, Raorane CJ, Shastri D, Raj V, Singh A, Kim SC. Update on modified chitosan frameworks and their applications for food, wastewater, toxic heavy metals, dyes treatment and cancer drug delivery. Journal of Environmental Chemical Engineering. 2022;10(6):108656.
15. Sethi S, Kaith BS. A review on chitosan-gelatin nanocomposites: Synthesis, characterization and biomedical applications. Reactive and Functional Polymers. 2022;179:105362.
16. Raval M, Patel P, Airao V, Bhatt V, Sheth N. Novel silibinin loaded chitosan-coated PLGA/PCL nanoparticles based inhalation formulations with improved cytotoxicity and bioavailability for lung cancer. Bionanoscience. 2021;11:67-83.
17. Samy M, Abdallah HM, Awad HM, Ayoub MM. In vitro release and cytotoxicity activity of 5-fluorouracil entrapped polycaprolactone nanoparticles. Polymer Bulletin. 2022:1-27.
18. Sukhanova TyEe, Vylegzhanina M, Volkov AY, Gasilova ER, Kutin AA, Samy M, et al. Comparative Study of Polymer Nanoparticles on the Basis of Caprolactone–Polyvinyl Alcohol Mixtures with an Encapsulated Antitumor Preparation by Atomic Force Microscopy, X-Ray Diffraction, and Dynamic Light Scattering. Technical Physics. 2019;64:1729-37.
19. Samy M, Abdallah HM, Ayoub MM, Vylegzhanina M, Volkov AY, Sukhanova T. Eco-friendly route for encapsulation of 5-fluorouracil into polycaprolactone nanoparticles. Egyptian Journal of Chemistry. 2020;63(1):255-67.
20. Ignjatović N, Wu V, Ajduković Z, Mihajilov-Krstev T, Uskoković V, Uskoković D. Chitosan-PLGA polymer blends as coatings for hydroxyapatite nanoparticles and their effect on antimicrobial properties, osteoconductivity and regeneration of osseous tissues. Materials Science and Engineering: C. 2016;60:357-64.
21. Zheng F, Wang S, Wen S, Shen M, Zhu M, Shi X. Characterization and antibacterial activity of amoxicillin-loaded electrospun nano-hydroxyapatite/poly (lactic-co-glycolic acid) composite nanofibers. Biomaterials. 2013;34(4):1402-12.
22. Marcano RGdJV, Tominaga TT, Khalil NM, Pedroso LS, Mainardes RM. Chitosan functionalized poly (ε-caprolactone) nanoparticles for amphotericin B delivery. Carbohydrate polymers. 2018;202:345-54.
23. Basha M, Hosam Abd El-Alim S, Alaa Kassem A, El Awdan S, Awad G. Benzocaine loaded solid lipid nanoparticles: formulation design, in vitro and in vivo evaluation of local anesthetic effect. Current drug delivery. 2015;12(6):680-92.
24. Samy M, Ekram B, Abd El-Hady BM, Ayoub MM. In vitro release study of electrospun poly (ε-caprolactone)/gelatin nanofiber mats loaded with 5-fluorouracil. Polymer Bulletin. 2024;81(5):3953-72.
25. Khrushchev AY, Akmaev E, Gulyaeva AY, Likhikh T, Khodkova J, Kolyachkina S. Quantitative measurement of trace amoxicillin using SERS under the conditions of controlled agglomeration of silver nanoparticles. Vibrational Spectroscopy. 2022;120:103388.
26. Imanipoor J, Mohammadi M, Dinari M, Ehsani MR. Adsorption and desorption of amoxicillin antibiotic from water matrices using an effective and recyclable MIL-53 (Al) metal–organic framework adsorbent. Journal of Chemical & Engineering Data. 2020;66(1):389-403.
27. Al-Nemrawi NK, Alshraiedeh NAH, Zayed AL, Altaani BM. Low molecular weight chitosan-coated PLGA nanoparticles for pulmonary delivery of tobramycin for cystic fibrosis. Pharmaceuticals. 2018;11(1):28.

28. Badran MM, Alomrani AH, Harisa GI, Ashour AE, Kumar A, Yassin AE. Novel docetaxel chitosan-coated PLGA/PCL nanoparticles with magnified cytotoxicity and bioavailability. Biomedicine & pharmacotherapy. 2018;106:1461-8.
29. Mazzarino L, Loch-Neckel G, Bubniak LdS, Mazzucco S, Santos-Silva MC, Borsali R, et al. Curcumin-loaded chitosan-coated nanoparticles as a new approach for the local treatment of oral cavity cancer. Journal of nanoscience and nanotechnology. 2015;15(1):781-91.
30. Akhtar B, Muhammad F, Aslam B, Saleemi MK, Sharif A. Pharmacokinetic profile of chitosan modified poly lactic co-glycolic acid biodegradable nanoparticles following oral delivery of gentamicin in rabbits. International Journal of Biological Macromolecules. 2020;164:1493-500.
31. Prasanna A, Venkatasubbu GD. Sustained release of amoxicillin from hydroxyapatite nanocomposite for bone infections. Progress in biomaterials. 2018;7:289-96.
32. Gaber DA, Alhawas HS, Alfadhel FA, Abdoun SA, Alsubaiyel AM, Alsawi RM. Mini-tablets versus nanoparticles for controlling the release of amoxicillin: In vitro/in vivo study. Drug design, development and therapy. 2020:5405-18.
33. Mirzaeei S, Mansurian M, Asare-Addo K, Nokhodchi A. Metronidazole-and amoxicillin-loaded PLGA and PCL nanofibers as potential drug delivery systems for the treatment of periodontitis: in vitro and in vivo evaluations. Biomedicines. 2021;9(8):975.
34. Samy M, Abd El-Alim SH, Amin A, Ayoub MM. Formulation, characterization and in vitro release study of 5-fluorouracil loaded chitosan nanoparticles. International journal of biological macromolecules. 2020;156:783-91.
35. Gaur M, Maurya S, Akhtar MS, Yadav AB. Synthesis and Evaluation of BSA-Loaded PLGA–Chitosan Composite Nanoparticles for the Protein-Based Drug Delivery System. ACS omega. 2023;8(21):18751-9.
36. Singh M, Chauhan D, Gill R, Iqbal Z, Solanki P. Sustained release of drug loaded nanofibers for wound dressing applications. Indian Journal of Biochemistry and Biophysics (IJBB). 2022;59(4):479-85.
37. Zhang Y, Yang Y, Tang K, Hu X, Zou G. Physicochemical characterization and antioxidant activity of quercetin-loaded chitosan nanoparticles. Journal of Applied Polymer Science. 2008;107(2):891-7.
38. Samy M, Abdallah HM, Awad HM, Ayoub MM. Preparation, Characterization and In vitro Biological activity of 5-Fluorouracil Loaded onto poly (D, L-lactic-co-glycolic acid) Nanoparticles. Polymer Bulletin. 2023;80(6):6197-219.
39. Tummala S, Kumar MS, Prakash A. Formulation and characterization of 5-Fluorouracil enteric coated nanoparticles for sustained and localized release in treating colorectal cancer. Saudi Pharmaceutical Journal. 2015;23(3):308-14.
40. Arafa MG, Mousa HA, Afifi NN. Preparation of PLGA-chitosan based nanocarriers for enhancing antibacterial effect of ciprofloxacin in root canal infection. Drug Delivery. 2020;27(1):26-39.
41. Guo Y, Shalaev E, Smith S. Physical stability of pharmaceutical formulations: solid-state characterization of amorphous dispersions. TrAC Trends in Analytical Chemistry. 2013;49:137-44.
42. Maswadeh H. Incompatibility of paracetamol with pediatric suspensions containing amoxicillin, azithromycin and cefuroxime axetil. Pharmacology & Pharmacy. 2017;8(11):355.
43. León FC, Lizardi-Mendoza J, Argüelles-Monal W, Carvajal-Millan E, Franco YL, Goycoolea F. Supercritical CO 2 dried chitosan nanoparticles: production and characterization. RSC advances. 2017;7(49):30879-85.
44. Silva ATCR, Cardoso BCO, e Silva MESR, Freitas RFS, Sousa RG. Synthesis, characterization, and study of PLGA copolymer in vitro degradation. Journal of Biomaterials and Nanobiotechnology. 2015;6(01):8.
45. Öztürk AA, Kıyan HT. Treatment of oxidative stress-induced pain and inflammation with dexketoprofen trometamol loaded different molecular weight chitosan nanoparticles: Formulation, characterization and anti-inflammatory activity by using in vivo HET-CAM assay. Microvascular Research. 2020;128:103961.
46. Baghirova L, Kaya Tilki E, Ozturk AA. Evaluation of cell proliferation and wound healing effects of vitamin A palmitate-loaded PLGA/chitosan-coated PLGA nanoparticles: Preparation, characterization, release, and release kinetics. ACS omega. 2023;8(2):2658-68.